

Proton NMR: spin-spin relaxation time dependency on pH

Author: Manuel Pereda Ávila.

Facultat de Física, Universitat de Barcelona, Diagonal 645, 08028 Barcelona, Spain.

Advisor: Ferran Macia Bros

(Dated: 05/07/2024)

Abstract: The current research investigates the phenomena of nuclear magnetic resonance (NMR) of the hydrogen nuclei. The experimental results on spin-spin relaxation times (T_2^*) using a Pulsed/CW NMR Spectrometer over samples with different pH, (concentration of Hydrogen ions) are discussed providing information on magnetization dynamics and decay profiles. While observed discrepancies exist, associations between T_2^* and proton density offer important clues about different pH samples behaviors in magnetic resonance.

I. INTRODUCTION

Nuclear Magnetic Resonance (NMR) is a powerful tool for studying nuclear-level processes, particularly those involving magnetic systems with angular momentum. The hydrogen nucleus exhibits a magnetic moment μ and an angular momentum J , which can be described as parallel:

$$\mu = \gamma \mathbf{J}, \quad (1)$$

where γ represents a scalar quantity called the "gyromagnetic ratio". The total magnetic and angular momentum are calculable from the wave function of a given nucleus state [1].

It is defined a dimensionless angular momentum operator \mathbf{I} by the equation:

$$\mathbf{J} = \hbar \mathbf{I}. \quad (2)$$

The eigenvalues of \mathbf{I}^2 are $I(I+1)$, where I is either integer or half-integer. Any component of \mathbf{I} , i.e., I_z , commutes with \mathbf{I}^2 , so we may simultaneously specify eigenvalues of \mathbf{I}^2 and I_z . The eigenvalues are $I(I+1)$ and $m = \{-I, -I+1, \dots, I\}$, respectively.

When a magnetic field \mathbf{H} is applied, an interaction energy, the Zeeman energy, is produced for the nucleus amounting to $-\mu \cdot \mathbf{H}$. Therefore, the Hamiltonian may be written as:

$$\mathcal{H} = -\mu \cdot \mathbf{H}. \quad (3)$$

Assuming the field to be H_0 along the z -direction and taking equations (1) and (2) into account, we find

$$\mathcal{H} = -\gamma \hbar H_0 I_z. \quad (4)$$

The eigenvalues of this Hamiltonian then are

$$E = -\gamma \hbar H_0 m. \quad (5)$$

For Hydrogen, $I = \frac{1}{2}$. These energy levels, known as Zeeman levels, are illustrated in Fig. 1.

An interaction is needed to cause transitions between Zeeman levels. To satisfy the conservation of energy, the interaction must be time-dependent with a frequency ω_0 matching the energy difference between levels, as follows:

$$\hbar \omega_0 = \Delta E, \quad (6)$$

where ΔE is the energy difference between Zeeman levels.

When an alternating magnetic field of amplitude H_x^1 is applied perpendicular to the static field H_0 , we get a perturbing term in the Hamiltonian of

$$\mathcal{H}_{\text{pert}} = -\gamma \hbar H_x^1 I_x \cos(\omega_0 t). \quad (7)$$

Consequently, the allowed transitions are between adjacent energy levels, giving [2]

$$\hbar \omega_0 = \Delta E = \gamma \hbar H_0, \quad (8)$$

or

$$\omega_0 = \gamma H_0. \quad (9)$$

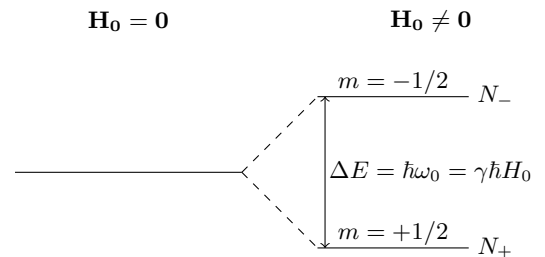


FIG. 1: Zeeman levels of Eq. (4) for $I = 1/2$.

For a large sample of N nuclei, we specify the number in the two m available states, $+1/2$ and $-1/2$, by N_+ and N_- , respectively. Of course, $N = N_+ + N_-$ [3].

The population ratio in thermal equilibrium is given by the Boltzmann factor:

$$\frac{N_-}{N_+} = e^{\frac{\Delta E}{kT}} = e^{\frac{\hbar \omega_0}{kT}}, \quad (10)$$

where k is the Boltzmann constant and T the temperature. The magnetization in the z -axis is then

$$M_z = \mu(N_+ - N_-). \quad (11)$$

The thermal equilibrium magnetization for N magnetic moments is

$$M_0 = N\mu \tanh\left(\frac{\mu H_0}{kT}\right). \quad (12)$$

Our focus is on the magnetization within the x - y plane. Under thermal equilibrium conditions, the sample exhibits a net magnetization only along the z -axis, denoted as M_z , which is aligned with the external magnetic field. In a classical frame, we can imagine a series of current loops situated in a magnetic field \mathbf{H}_0 . The torque $\boldsymbol{\tau}$ exerted on these loops leads to a change in their angular momentum, as expressed by:

$$\boldsymbol{\tau} = \boldsymbol{\mu} \times \mathbf{H}_0 = \frac{d\mathbf{J}}{dt}. \quad (13)$$

For the nuclei, Eq. (13) becomes

$$\boldsymbol{\mu} \times \mathbf{H}_0 = \frac{1}{\gamma} \frac{d\boldsymbol{\mu}}{dt}. \quad (14)$$

Eq. (14) shows that the magnetic moment will execute precessional motion with precessional frequency $\omega_0 = \gamma H_0$, which is the resonant frequency in Eq. (9).

For the x -components of each nucleus to contribute to a net M_x , the precessing spins must be in phase. In thermal equilibrium, the spin components in the x - y plane are randomly oriented, resulting in no net transverse (x or y) magnetization. However, it is possible to generate transverse magnetization using radiofrequency pulsed magnetic fields. This method involves rapidly rotating the equilibrium magnetization M_z into the x - y plane, thereby creating temporary M_x and M_y components.

Equation (14) can be extended to describe the classical motion of the net magnetization for the entire sample:

$$\frac{d\mathbf{M}}{dt} = \gamma \mathbf{M} \times \mathbf{H}, \quad (15)$$

where \mathbf{H} represents any magnetic field.

Now, consider applying both a constant magnetic field $H_0 \hat{\mathbf{k}}$ and a rotating (circularly polarized) magnetic field with angular frequency ω in the x - y plane, so the total field is expressed as:

$$\mathbf{H}(t) = H_1 \cos(\omega t) \hat{\mathbf{i}} + H_1 \sin(\omega t) \hat{\mathbf{j}} + H_0 \hat{\mathbf{k}} \quad (16)$$

To simplify, we choose a rotating coordinate system where the rotating magnetic field appears stationary and aligned along the x^* axis (see Fig. 2). In this rotating

frame, \mathbf{H}_0 and \mathbf{H}_1 are not the only fields present. An effective field \mathbf{H}_{eff} along the z^* axis must also be considered. The total magnetic field in the rotating frame is depicted in Fig. ?? and is given by [4]:

$$\mathbf{H}_{\text{eff}}^* = H_1 \hat{\mathbf{i}}^* + \left(H_0 - \frac{\omega}{\gamma}\right) \hat{\mathbf{k}}^*. \quad (17)$$

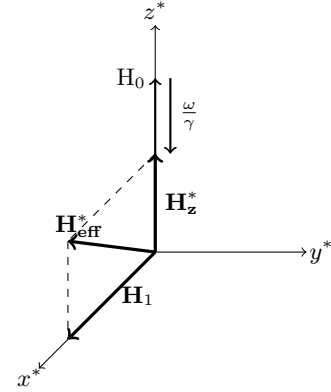


FIG. 2: Effective magnetic field $\mathbf{H}_{\text{eff}}^*$ in the rotating coordinate system.

According to Eq. (15), in the rotating frame, \mathbf{M} will precess around $\mathbf{H}_{\text{eff}}^*$.

When a rotating magnetic field with a frequency ω_0 such that $\omega_0 = \gamma H_0$ is applied, $\mathbf{H}_{\text{eff}}^* = H_1 \hat{\mathbf{i}}^*$, forming a constant magnetic field in the x^* direction. As a result, M_z precesses around this magnetic field at a rate $\Omega = \gamma H_1$ in the rotating frame. If the H_1 field is turned off when the magnetization reaches the x - y plane, a non-equilibrium state is created, resulting in a net magnetization in the x - y plane. This net magnetization then precesses around $H_0 \hat{\mathbf{k}}$ and is detected by the spectrometer after the radiofrequency pulse.

However, in the rotating frame, the x - y magnetization will decay exponentially as described by:

$$\frac{dM_{x^*,y^*}}{dt} = -\frac{M_{x^*,y^*}}{T_2}. \quad (18)$$

The solution to this equation is:

$$M_{x^*,y^*} = M_0 e^{-\frac{t}{T_2}}, \quad (19)$$

where the characteristic decay time T_2 is known as the spin-spin relaxation time [6]. From a classical perspective, T_2 can be understood as each nucleus acting as a small magnet, generating a magnetic field that affects its neighbors. Consequently, for a given distribution of nuclei, there is a corresponding distribution of local magnetic fields, causing the nuclei to precess around $H_0 \hat{\mathbf{k}}$ with a range of frequencies.

From this analysis, it seems that the spin-spin relaxation time T_2 can be measured by plotting the decay of M_x (or M_y) following a $\pi/2$ pulse. This decay signal, known as free precession or free induction decay (FID), is indicative of T_2 . If the magnetic field were perfectly uniform throughout the sample volume, the decay time constant of the FID would indeed represent T_2 . However, in practice, the non-uniformity of the magnetic field over the sample typically determines the observed decay constant of the FID, referred to as T_2^* .

In this research, we propose that the value of T_2^* is strongly correlated with the proton concentration $[H^+]$, which is determined by the pH level [8, 9].

$$pH = -\log_{10}[H^+]. \quad (20)$$

We believe that varying pH levels may influence T_2^* by altering the magnetic interactions of hydrogen nuclei. Through experimentation and analysis of the FID of samples with different acidity levels, we aim to explore how these variations affect T_2^* . This investigation not only enhances our understanding of magnetic resonance phenomena but also has potential implications for optimizing MRI techniques in biomedical applications.

II. INSTRUMENTATION

TeachSpin's Pulsed/CW NMR Spectrometer PS2 is been used for the experimental study. It's components are the following [5]:

- A (0.50 ± 0.01) T NdFeB permanent magnet provides high stability and homogeneity, essential for precise measurements. It generates the constant z -axis magnetic field H_0 . The sample probe head includes an adjustable RCL circuit to match the frequency of the RF pulses.
- The receiver module amplifies the small voltage induced in the sample coil, which also generates the pulse at the sample, oriented along the y -axis. The envelope detector (Env. Out) tracks the amplitude of the input RF voltage, while the phase-sensitive detectors provide in-phase (I Out) and quadrature (Q Out) components, aiding in identifying the correct resonant frequency.
- The synthesizer module supplies the radio frequency (RF) signals for the spectrometer, capable of producing RF signals ranging from below 1 MHz to over 30 MHz.
- The pulse programmer module creates pulsed sequences, controlling the duration of the A and B pulses. In pulse mode, the RF pulse amplitude remains constant, so adjusting the pulse length achieves $\frac{\pi}{2}$ or π rotations of magnetization. In our

experiments, only single pulse experiments were conducted.

- An oscilloscope is used to visualize the signals from the Env. Out and I Out of the spectrometer.

III. RESULTS

Six samples of different pH values were prepared in order to measure its T_2^* . With the oscilloscope connected to the PS2 receiver, we were able to set the correct temperature-dependant resonant frequency to measure the FID. To do so, the I-out signal must match the Env. Out signal (see Fig.3) [7]. The pulse length that resulted in the most long FID, therefore a $\frac{\pi}{2}$ turn, was $1.12 \mu\text{s}$.

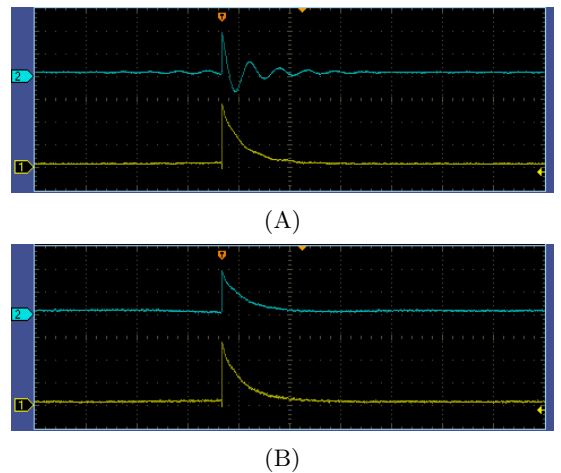


FIG. 3: Signal of Env. Out on channel 1 and I out over time on channel 2 seen on the oscilloscope screen. The time division is 4 ms. Image (A) shows the scenario in which the frequency doesn't match the resonant frequency by approximately 350 Hz. On the other hand, image (B) shows that we are on resonance.

Then, the envelope of the signal data was recorded over time to fit the best exponential decay to each FID (Eq. 19). The results for the decay constant was $(T_2^*)^{-1}$ then we could calculate T_2^* (see table I).

pH	$1/T_2^*$ (ms^{-1})	$\delta 1/T_2^*$ (ms^{-1})	T_2^* (ms)	δT_2^* (ms)
1	0.5886	0.0003	1.699	0.001
2	0.6163	0.0003	1.6225	0.0008
3	0.6439	0.0002	1.553	0.0005
4	0.6476	0.0002	1.5442	0.0005
5	0.6204	0.0002	1.6118	0.0006
7	0.6569	0.0002	1.5223	0.0006

TABLE I: Inverse of T_2^* given by the exponential fit and the calculated value of T_2^* with its errors associated with each pH value of the samples.

To gain insight, we plotted the signal envelope for the

six studies samples as a function of time (see Fig.4); in (A) during the first 2 ms and in (B) from 2 to 4 ms. There seems to be two different behaviours over time. In (A) seems that pH 7 sample has the slowest decay while in (B) pH 1 is so.

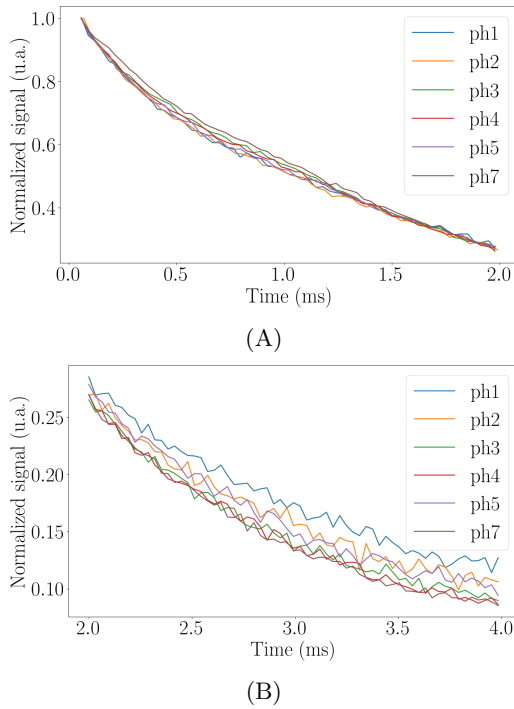


FIG. 4: FID signal normalized over time zoomed from 0 to 2 ms (A) and from 2 to 4 ms (B).

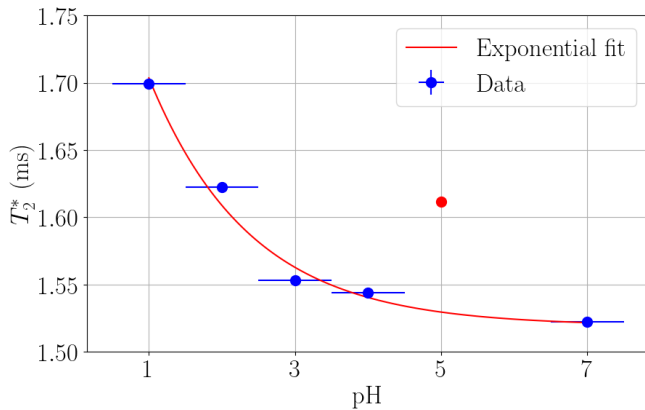


FIG. 5: T_2^* in terms of pH. The horizontal error bars correspond to the pH determination error, while the vertical error bars are so small that cannot be seen. The determination coefficient of the Eq. (21) $R^2 = 0.9848$.

$$T_2^* = 3.79 \times 10^{-1} e^{-7.22 \cdot \text{pH}} + 1.52 \text{ (ms)}. \quad (21)$$

The errors of the parameters of Eq. (21) are

$$\delta a = 0.03 \times 10^{-1} \text{ ms}, \delta b = 0.00 \text{ and } \delta c = 0.01 \text{ ms}.$$

The results that shows on table I were plotted (see fig.5) to analyze if they were somehow correlated. It's been found that a $a \exp(bt) + c$ exponential regression correlates adequately with the data. In any case, data corresponding to pH = 5 was not considered to fit the exponential regression.

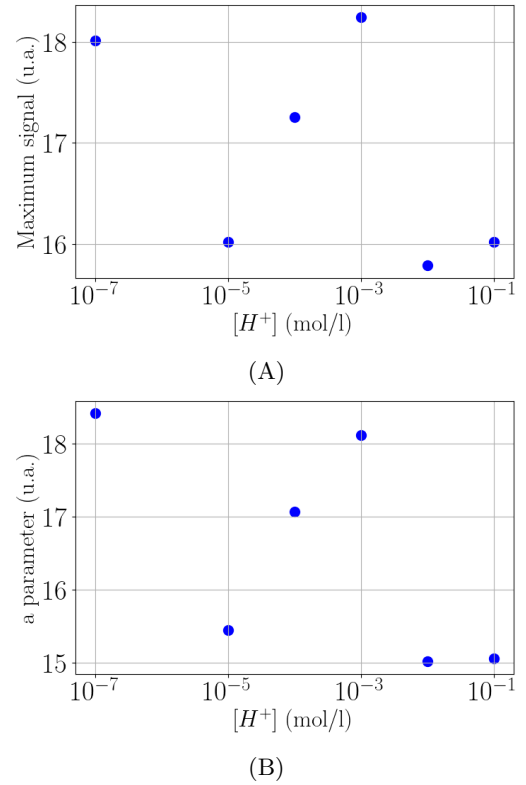


FIG. 6: Maximum signal given by the oscilloscope (A) and a parameter of the exponential regression (B) in terms of proton concentration $[H^+]$ of the sample in a logarithmic x-axis.

pH	$[H^+]$ (mol/l)	Max. Signal (u.a.)	a parameter	δa
1	10^{-1}	16.020	15.058	0.006
2	10^{-2}	15.791	15.018	0.005
3	10^{-3}	18.242	18.117	0.004
4	10^{-4}	17.254	17.066	0.004
5	10^{-5}	16.025	15.449	0.004
7	10^{-7}	18.012	18.415	0.005

TABLE II: Proton concentration $[H^+]$, maximum signal value, a parameter of the exponential regression and its for each pH.

Besides this, the maximum signal value has been examined. Two plots have been made. The first one (A) plots the maximum signal value against the proton density $[H^+]$ related to pH by Eq. (20).

The second one (B) plots the a parameter of the exponential regression for the FID of each sample dependence on $[H^+]$. The a parameter of the exponential regression is related to M_0 by Eq. (19). Despite this, no correlation was found.

IV. CONCLUSIONS

The study of the FID of the six different acidity samples has leas us to the next conclusions.

First, it is been found an exponential regression that fits the T_2^* data (Fig.5). Despite that, only five points were used to fit this adjust. Nevertheless, it looks like T_2^* decreases with pH according to the Eq. (20). This might lead us to think that T_2^* increases with proton density.

Second, Fig.4 reflects an inversion of decay times around 1.5 ms. The first tendency decays quickly compared to the second one, which dominates for times greater than 2 ms. The tendency that dominates the first 1.5 ms is attributed to the experimental setup.

Furthermore, Fig.6 shows no clear correlation between the maximum signal that the sample gives after the RF pulse and the proton concentration $[H^+]$ of the different

samples.

In conclusion, pH of the sample seems to correlate exponentially with the T_2^* . To improve this results on further research, two pulse experiments [10] could be done to clarify this fact. More and better prepared samples would help on ensuring the exponential regression and would lead to narrower error bars on the x -axis.

Acknowledgments

I am so grateful to my mentor, Ferran Macia, for his very useful advice and support in this study. It's pertinent to mention that I have always received his appropriate professional advice and encouragement whenever I faced obstacles.

For a start, I would like to express deep gratitude towards Tarik Bada who provided extra insight into the research.

My family has been very supportive of my decisions over the years. In particular, special thanks go to my grand father whose deeply profound interest in physics have always been a source of inspiration ever since.

-
- [1] C.P. Slichter, *Principles of Magnetic Resonance*, Third Enlarged and Updated Edition, (Springer Series in Solid-State Sciences, vol. 1, Springer Berlin, Heidelberg, 1990), Sec. 2.2.
 - [2] C.P. Slichter, *Principles of Magnetic Resonance*, Third Enlarged and Updated Edition, (Springer Series in Solid-State Sciences, vol. 1, Springer Berlin, Heidelberg, 1990), Sec. 1.2.
 - [3] C.P. Slichter, *Principles of Magnetic Resonance*, Third Enlarged and Updated Edition, (Springer Series in Solid-State Sciences, vol. 1, Springer Berlin, Heidelberg, 1990), Sec. 1.3.
 - [4] TeachSpin, Inc., *Pulsed/CW NMR Spectrometer PS2-A/B/C Instructor's Manual*, TeachSpin, Inc., 2495 Main Street Suite 409, Buffalo, NY 14214-2153, p. I-8.
 - [5] TeachSpin, Inc., *Pulsed/CW NMR Spectrometer PS2-A/B/C Instructor's Manual*, TeachSpin, Inc., 2495 Main Street Suite 409, Buffalo, NY 14214-2153, sec. II.
 - [6] C.P. Slichter, *Principles of Magnetic Resonance*, Third Enlarged and Updated Edition, (Springer Series in Solid-State Sciences, vol. 1, Springer Berlin, Heidelberg, 1990), Sec. 2.7.
 - [7] TeachSpin, Inc., *Pulsed/CW NMR Spectrometer PS2-A/B/C Instructor's Manual*, TeachSpin, Inc., 2495 Main Street Suite 409, Buffalo, NY 14214-2153, p. III-6.
 - [8] Yves Gossuin, Aline Hocq, Pierre Gillis, Vuong Quoc Lam, *Physics of magnetic resonance imaging: from spin to pixel*, Journal of Physics D: Applied Physics **43** (2010), p. 10-11.
 - [9] Mark Jenkinson and Michael Chappell (Series editors), *Short introduction to MRI Physics for neuroimaging*, Oxford Neuroimaging Primers, Oxford University Press, p.9,14.
 - [10] C.P. Slichter, *Principles of Magnetic Resonance*, Third Enlarged and Updated Edition, (Springer Series in Solid-State Sciences, vol. 1, Springer Berlin, Heidelberg, 1990), Sec. 2.9.